J. Fluid Mech. (1997), *vol.* 353, *pp.* 357–381. Printed in the United Kingdom

Three-dimensional instability of viscoelastic elliptic vortices

By H. HAJ-HARIRI[1] AND G. M. HOMSY[2]

[1]Department of Mechanical and Aerospace Engineering, University of Virginia, Charlottesville, VA 22903, USA

[2]Department of Chemical Engineering, Stanford University, Stanford, CA 94305, USA

(Received 16 June 1997 and in revised form 27 August 1997)

An analysis of the three-dimensional instability of two-dimensional viscoelastic elliptical flows is presented, extending the inviscid analysis of Bayly (1986) to include both viscous and elastic effects. The problem is governed by three parameters: E, a geometric parameter related to the ellipticity; Re, a wavenumber-based Reynolds number; and De, the Deborah number based on the period of the base flow. New modes and mechanisms of instability are discovered. The flow is generally susceptible to instabilities in the form of propagating plane waves with a rotating wavevector, the tip of which traces an ellipse of the same eccentricity as the flow, but with the major and minor axes interchanged. Whereas a necessary condition for purely inertial instability is that the wavevector has a non-vanishing component along the vortex axis, the viscoelastic modes of instability are most prominent when their wavevectors *do* vanish along this axis. Our analytical and numerical results delineate the region of parameter space of (E, Re, De) for which the new instability exists. A simple model oscillator equation of the Mathieu type is developed and shown to embody the essential qualitative and quantitative features of the secular viscoelastic instability. The cause of the instability is a buckling of the 'compressed' polymers as they are perturbed transversely during a particular phase of the passage of the rotating plane wave.

1. Introduction

Understanding and controlling the physics of transition to turbulence in shear flows has been a vital area of research in fluid dynamics. The advent of advanced visualization methods and powerful computational capabilities has led to substantial progress over the last few years. The body of literature in the areas of free- and bounded-shear layer transition is immense and is reviewed periodically (e.g. Ho & Huerre 1984; Herbert 1988; Bayly, Orszag & Herbert 1988; Kachanov 1994). Whereas a number of active and passive means have been used to control the transition process in shear layers, our work is motivated by the fact that the addition of minute amounts of dissolved polymers to a flow can reduce turbulent drag drastically (cf. the early review by Berman 1978). The recent experiments of Bonn *et al.* (1993) show marked changes in the small-scale vortical nature of a turbulent flow upon the introduction of polymers. The formation of high-vorticity filaments is strongly suppressed, thus reducing the drag by lowering the rate of gen-

eration of large eddies that in turn dissipate energy through their cascade to smaller scales.

The present work aims to develop an understanding of the viscoelastic effect of polymers on the stability of two-dimensional eddies. These eddies might originate in a free-shear flow, a wall-bounded shear flow, or even a free vortex. For the sake of argument, and without loss of generality, we will take the origin of the eddies in our study to be a nonlinear evolving two-dimensional free-shear layer characterized by regions containing vorticity in the presence of linear strain. Viscoelastic effects on the linear stability of high-speed shear layers were first studied by Azaiez & Homsy (1994*a*) where it was demonstrated that two-dimensional travelling-wave disturbances were damped compared with their polymer-free counterparts. Simulations of the nonlinear two-dimensional problem (Azaiez & Homsy 1994*b*) have shown only minor modifications of the Newtonian behaviour. Given the experimental evidence for the turbulent drag reduction, it is clear that three-dimensional effects need to be included.

Our work focuses on a two-dimensional elliptic vortex as a prototype of a two-dimensional eddy. In a pair of companion articles, Pierrehumbert (1986) and Bayly (1986) demonstrated – computationally and analytically, respectively – elliptic vortices to be susceptible to violent three-dimensional inertial instabilities. These authors put forth the relevance of investigating a simple linear basic state as a model of much more complicated flows. It can be argued that most perturbed shear-layer type flows possess closed streamlines in a relevant frame of reference (i.e. Kelvin's cat's eye pattern). Near the core of such regions one may approximate the flow by the linear terms in a Taylor series expansion.

The present work extends the Floquet analysis of Bayly (1986) to allow for the inclusion of viscoelastic effects. Such effects are included through the use of the Oldroyd-B constitutive equation, described later. It is shown that one may still investigate the stability of the problem by searching the space of a special class of plane-wave solutions. Furthermore, we will show the effects of Newtonian viscosity on the stability of the elliptic vortex to be of secondary importance, and hence will retain only the viscoelastic terms in our stability analysis.

Hinch contributed an Appendix to Azaiez & Homsy (1994*a*) where he argued the role of the polymers in a high-speed shear flow to be equivalent to a membrane with surface tension. This explains the moderation of the growth rates observed by Azaiez & Homsy (1994*a*). However, there is always a band of long waves that are too long to feel the effects of the membrane, and they grow. Their growth will lead to the development of two-dimensional eddies whose inertial stability was studied by Pierrehumbert (1986) and Bayly (1986), and whose viscoelastic instability is the subject of the present work.

The problem formulation and the governing equations are presented in §2. The flow field and the viscoelastic stress distribution for the base elliptic vortex are obtained in §3. In §4 we present the linear-stability formulation for this base flow, and provide the rudiments of Floquet analysis needed to obtain the dispersion relations. Section 5 contains a comprehensive set of results of our stability analysis; in particular, we discover a *new* viscoelastic mode of instability. In §6 we perform a term-by-term interrogation of the linear-stability equations, develop and solve a model oscillator equation, and subsequently provide a mathematical and physical mechanism for the new instability mentioned above. Section 6 also contains our brief concluding remarks.

2. Problem definition and basic equations

The elliptic vortex is a two-dimensional flow in the (x, y)-plane with elliptic streamlines characterized by the rotational frequency Ω and a geometric parameter E, and having the velocity field

$$\boldsymbol{U}(x, y) = (U, V, 0) = \Omega \left(-Ey, \frac{1}{E}x, 0 \right), \quad E > 1. \tag{1}$$

The parameter E is that introduced by Bayly (1986). Even though it is not the geometric eccentricity of the elliptic streamlines, we will refer to it as the 'eccentricity'. The vorticity and shear for this flow are uniform. The vortex extends to infinity (unlike a Rankine vortex for example) and hence does not turn over under its own induced velocity (cf. Batchelor 1967, p. 534). The elliptic flow can be considered as a local view of the core of the Kelvin cat's eye pattern as seen, for example, by an observer moving at the phase speed of a transverse wave propagating along a free shear layer, and is therefore a prototype of a wide class of two-dimensional shear flows. Furthermore, by varying the eccentricity of this flow one may simulate a nonlinearly perturbed shear layer, whose stability can then be studied. Such studies can shed light on the evolution of shear layers and on the ultimate fate of instabilities, i.e. whether they saturate or not.

Our interest is in such elliptic vortices when the fluid is viscoelastic. In choosing an appropriate constitutive model for such a fluid, an important consideration is the presence or absence of stagnation points. Such points exist for example at the intersections of the separatrices of the Kelvin cat's eye pattern, or those of Stuart vortices (cf. Stuart 1967). These points appear as saddle points on the streamline plot. The vanishing of vorticity at a stagnation point allows the polymers to be aligned with the principal stretch direction and to develop large stretch due to the infinitely long time scales existing near a stagnation point – a phenomenon which persists so long as the vorticity is less than the strain rate locally. A linearly viscoelastic model assumes a Hookean spring connecting two beads, and would predict infinite stresses under such unbounded extensions. Azaiez & Homsy (1994*b*) noticed this problem in their simulations of the nonlinearly evolving shear layer. The correct approach is to include finite extensibility of the springs into the model and use the so-called finitely extensible nonlinearly elastic (FENE) constitutive model for the polymers. The elliptic flow has no zero-vorticity stagnation points, so these considerations are absent and constitutive equations of the Oldroyd type are appropriate.

The governing equations for the incompressible flow under investigation are the Cauchy momentum equation

$$\frac{\mathrm{d}\boldsymbol{u}}{\mathrm{d}t} = -\nabla p + \nabla \cdot \boldsymbol{\tau} + \rho \boldsymbol{f}, \tag{2}$$

and the continuity equation

$$\nabla \cdot \boldsymbol{u} = 0\,. \tag{3}$$

In these equations, p is the pressure, $\boldsymbol{\tau}$ is the total extra-stress tensor, and $\boldsymbol{f}$ is a body force which is usually needed to balance the equation when the flow is prescribed. As we will see, however, the elliptic flow has the advantage that it satisfies the momentum equation exactly, without the need for any compensating body forces. The extra stress $\boldsymbol{\tau}$ has a contribution from the viscosity of the solvent, η_s, and one from that of the polymer, η_p. The extra stress is decomposed into its Newtonian and polymer contributions as follows:

$$\boldsymbol{\tau} = \boldsymbol{\tau}^s + \boldsymbol{\tau}^p = \eta_s \dot{\boldsymbol{\gamma}} + \eta_p \boldsymbol{a} \equiv \eta \left[\kappa \dot{\boldsymbol{\gamma}} + \bar{\kappa} \boldsymbol{a} \right], \tag{4}$$

Name	Symbol	Definition
Eccentricity	E	—
Viscosity ratio	κ	$\eta_s/(\eta_s+\eta_p)$
Reynolds number	Re	$\rho\Omega/(\eta k_o^2)$
Deborah number	De	$\lambda\Omega$
Wave inclincation	θ	$\min(\cos^{-1}(\boldsymbol{e}_z\cdot\hat{\boldsymbol{k}}))$

TABLE 1. The governing parameters

where $\kappa=\eta_s/\eta$ (with $\eta\equiv\eta_s+\eta_p$), $\bar{\kappa}=1-\kappa$, and (twice) the strain rate of the flow, $\nabla\boldsymbol{u}+(\nabla\boldsymbol{u})^T$, is denoted by $\dot{\boldsymbol{\gamma}}$. The extra-stress tensor for the polymers is linearly related to $\boldsymbol{a}$, the evolution of which is governed by the Oldroyd-B constitutive relation (cf. Bird *et al.* 1987):

$$\frac{\partial\boldsymbol{a}}{\partial t}+\boldsymbol{u}\cdot\nabla\boldsymbol{a}-(\boldsymbol{a}\cdot\nabla\boldsymbol{u}+(\nabla\boldsymbol{u})^T\cdot\boldsymbol{a})+\frac{1}{\lambda}(\boldsymbol{a}-\dot{\boldsymbol{\gamma}})=0, \tag{5}$$

where λ denotes the relaxation time for the polymers.

We shall now identify the appropriate scales for non-dimensionalizing the equations. The main time scale of the problem is the turnover period of the flow, Ω^{-1}. Selection of the length scale is not as straightforward. There are no scales arising from the geometry; this was evident from the self-similar nature of the inviscid solutions obtained by Bayly (1986) for this flow. The viscous (Newtonian) diffusion length is a potential candidate. However, our focus is on the effects of elasticity on the inertial instability of the base flow. Therefore, it is not advisable to use the viscous-diffusion scale as a length scale. Anticipating the stability analysis below, we will use the inverse of a norm of the wavevector ($k_o=\min|\boldsymbol{k}(t)|$) of the perturbations to define a length scale for the problem. Thus the derived scales for the velocity, pressure, and stresses (viscous and polymer) are Ω/k_o, $\rho\Omega^2/k_o^2$, and $\eta\Omega$, respectively. The resulting governing parameters for the problem are given in table 1.

The dynamic parameters Re and De denote ratios of various length and time scales, respectively. The former is the square of the ratio of the wavelength, k_o^{-1}, to the viscous diffusion length $(\eta/(\Omega\rho))^{1/2}$, while the latter is the ratio of the relaxation time scale of the polymer to the turnover time scale of the flow. The inclination parameter is introduced at this stage whereas it is used in §4 where we introduce disturbances to the basic state; it indicates the angle of closest approach of the time-dependent wavevector to the axis of the vortex.

3. Basic state

In this section we develop expressions for the basic-state velocity and polymer strain rates. Upper-case letters are used to denote basic-state variables, and lower-case letters are used to denote linear perturbations.

3.1. *Velocity field*

Consider the following (dimensionless) basic-state velocity field:

$$\boldsymbol{U}(x,y)=(U,V,0)=\left(-Ey,\frac{1}{E}x,0\right),\quad E>1, \tag{6}$$

which may be written as

$$\boldsymbol{U} = \Omega \boldsymbol{x}, \quad \Omega_{ij} = \begin{bmatrix} 0 & -E & 0 \\ E^{-1} & 0 & 0 \\ 0 & 0 & 0 \end{bmatrix} = \frac{1}{E}\delta_{i2}\delta_{j1} - E\delta_{i1}\delta_{j2}. \tag{7}$$

For this *linear* basic state, the velocity-gradient tensor is then constant:

$$\nabla \boldsymbol{U} = \frac{\partial u_j}{\partial x_i}\boldsymbol{e}_i\boldsymbol{e}_j = \Omega_{jk}\delta_{ik}\boldsymbol{e}_i\boldsymbol{e}_j = \Omega_{ji}\boldsymbol{e}_i\boldsymbol{e}_j = \Omega^T. \tag{8}$$

The rate-of-strain tensor, $\dot{\Gamma}$, is then also constant:

$$\dot{\Gamma} = \nabla \boldsymbol{U} + (\nabla \boldsymbol{U})^T = (\Omega^T + \Omega)$$

$$\Rightarrow \quad [\dot{\Gamma}_{ij}] = \left(\frac{1}{E} - E\right)\begin{bmatrix} 0 & 1 & 0 \\ 1 & 0 & 0 \\ 0 & 0 & 0 \end{bmatrix} \equiv \dot{\Gamma}\begin{bmatrix} 0 & 1 & 0 \\ 1 & 0 & 0 \\ 0 & 0 & 0 \end{bmatrix} = \dot{\Gamma}(\delta_{i1}\delta_{j2} + \delta_{i2}\delta_{j1}), \tag{9}$$

where $\dot{\Gamma} < 0$ since $E > 1$. For completeness, the constant vorticity of this flow is given as

$$\boldsymbol{\omega} = \nabla \wedge \boldsymbol{U} = \left(E + \frac{1}{E}\right)\boldsymbol{e}_z. \tag{10}$$

Note that the circular vortex $E = 1$ results in a rigid-body rotation with $\boldsymbol{\omega} = 2\boldsymbol{e}_z$ and $\dot{\Gamma} \equiv 0$, and thus E is a measure of the degree of strain in the base state.

Owing to the absence of viscous stress gradients, the basic state chosen above satisfies the Euler *and* Navier–Stokes equations. The objective here is to: (i) determine the basic-state polymer or extra-stress distribution, and (ii) perform an analysis of the stability of this augmented basic state so as to determine the effect of the extra stress and viscoelasticity on the evolution of three-dimensional disturbances.

In general the inclusion of viscoelasticity necessitates the addition of a body force in order to keep the velocity profile, $\boldsymbol{U}$, a solution of the Cauchy momentum equation:

$$\frac{\mathrm{d}\boldsymbol{U}}{\mathrm{d}t} = -\nabla P + \nabla \cdot \boldsymbol{T} + \boldsymbol{F}, \tag{11}$$

where

$$\boldsymbol{T} = \boldsymbol{T}^s + \boldsymbol{T}^p = \frac{1}{Re}[\kappa\dot{\Gamma} + (\bar{\kappa})\boldsymbol{A}]. \tag{12}$$

Therefore the basic-state extra-stress term which needs to be balanced by the body force is

$$\nabla \cdot \boldsymbol{T}^s = \frac{\bar{\kappa}}{Re}\nabla \cdot \boldsymbol{A}. \tag{13}$$

Thus as long as $\nabla \cdot \boldsymbol{A} = O(1)$ it is admissible to neglect this body force on the grounds that the viscosity of the flow is low and the important dynamics are essentially inviscid (cf. Azaiez & Homsy 1994*a*). However, as was mentioned above, and will be shown below, $\nabla \cdot \boldsymbol{T}$ is identically zero, so that there is no need for fictitious body forces to balance the equation.

3.2. *Polymer stress*

As justified above, we adopt the Oldroyd-B constitutive equation to relate the evolution of the rate-of-strain tensor for the polymer, $\boldsymbol{A}$, to the rate-of-strain tensor for

the flow, $\dot{\Gamma}$. The constitutive equation reads

$$\frac{\partial \boldsymbol{A}}{\partial t} + \boldsymbol{U}\cdot\nabla\boldsymbol{A} - (\boldsymbol{A}\cdot\nabla\boldsymbol{U} + (\nabla\boldsymbol{U})^T\cdot\boldsymbol{A}) + \frac{1}{De}(\boldsymbol{A} - \dot{\Gamma}) = 0, \tag{14}$$

where De is the Deborah number defined in table 1.

The governing equation (14) is hyperbolic. Therefore the PDE may be written as the following system of ODEs:

$$\frac{\mathrm{d}}{\mathrm{d}t}\boldsymbol{A} + \frac{1}{De}\boldsymbol{A} - (\boldsymbol{A}\cdot\Omega^T + \Omega\cdot\boldsymbol{A}) = \frac{\dot{\Gamma}}{De}, \tag{15}$$

on the particle trajectories

$$\frac{\mathrm{d}\boldsymbol{x}(t)}{\mathrm{d}t} = \boldsymbol{U} \qquad \Rightarrow \qquad \frac{\mathrm{d}x}{\mathrm{d}t} = -Ey, \qquad \frac{\mathrm{d}y}{\mathrm{d}t} = \frac{x}{E}. \tag{16}$$

The above equations state the evolution of $\boldsymbol{A}$ recognizing that the fluid particle is constrained to the streamlines

$$x^2 + E^2y^2 = \xi^2 = \text{const.} \qquad \text{or} \qquad x(t) = \xi\cos(t), \quad y(t) = \frac{\xi}{E}\sin(t). \tag{17}$$

Note that by our choice of time scaling, the period of completing one orbit along any streamline is 2π. The ODE for $\boldsymbol{A}$ is expanded as follows:

$$\frac{\mathrm{d}}{\mathrm{d}t}A_{ij} + \frac{1}{De}A_{ij} - \left[\frac{1}{E}A_{i1}\delta_{j2} - EA_{i2}\delta_{j1} + \frac{1}{E}A_{1j}\delta_{i2} - EA_{2j}\delta_{i1}\right] = \frac{\dot{\Gamma}}{De}(\delta_{i2}\delta_{j1} + \delta_{i1}\delta_{j2}). \tag{18}$$

It can be shown that A_{i3} are decoupled from the other components of $\boldsymbol{A}$, and are governed by a homogeneous system so that these components vanish once the transients have subsided. Therefore, one need consider only the reduced system for A_{ij} with i and j different from 3, in order to obtain the non-trivial steady-state polymer-stress components. This reduced system reads

$$\frac{\mathrm{d}}{\mathrm{d}t}\boldsymbol{A} + \frac{1}{De}\boldsymbol{A} - \begin{bmatrix} -E(A_{12}+A_{21}) & \frac{1}{E}A_{11} - EA_{22} \\ -EA_{22} + \frac{1}{E}A_{11} & \frac{1}{E}(A_{21}+A_{12}) \end{bmatrix} = \frac{\dot{\Gamma}}{De}\begin{bmatrix} 0 & 1 \\ 1 & 0 \end{bmatrix}. \tag{19}$$

Noting the symmetry of the tensor $\boldsymbol{A}$, the following system of equations needs be solved for the three unknown components A_{11}, A_{22}, and A_{12}:

$$\frac{\mathrm{d}}{\mathrm{d}t}\begin{Bmatrix} A_{11} \\ A_{22} \\ A_{12} \end{Bmatrix} = \begin{bmatrix} -\frac{1}{De} & 0 & -2E \\ 0 & -\frac{1}{De} & \frac{2}{E} \\ \frac{1}{E} & -E & -\frac{1}{De} \end{bmatrix}\begin{Bmatrix} A_{11} \\ A_{22} \\ A_{12} \end{Bmatrix} + \begin{Bmatrix} 0 \\ 0 \\ \frac{\dot{\Gamma}}{De} \end{Bmatrix}. \tag{20}$$

The solution of the above system exhibits a decaying transient – with time dependence of the form $\exp\{-t/De\}$ – through which the general initial conditions approach the steady-state solution given as the particular solution of the above system:

$$\begin{Bmatrix} A_{11} \\ A_{22} \\ A_{12} \end{Bmatrix} = \frac{\dot{\Gamma}}{1+4De^2}\begin{Bmatrix} -2E\ De \\ 2De/E \\ 1 \end{Bmatrix}. \tag{21}$$

The normal stress differences, resolved in the Cartesian coordinates, are given as

$$A_{11} - A_{22} = \frac{2De}{1 + 4De^2}\left(E^2 - \frac{1}{E^2}\right) > 0, \tag{22}$$

$$A_{22} - A_{33} = -\frac{2De}{1 + 4De^2}\left(1 - \frac{1}{E^2}\right) < 0, \tag{23}$$

where we have used the definition $\dot{\Gamma} = (1/E - E)$. We note that $\nabla \cdot \boldsymbol{A} \equiv 0$, and therefore the viscoelastic elliptical vortex for our Oldroyd-B fluid is an exact solution of the basic equations.

4. Linear stability

In this section we consider the linear stability of the basic state derived above. The linearized equations governing the evolution of small disturbances, denoted in lower-case letters, are

$$(\partial_t + \boldsymbol{U} \cdot \nabla)\boldsymbol{u} + \boldsymbol{u} \cdot \nabla \boldsymbol{U} = -\nabla p + \frac{\kappa}{Re}\nabla^2 \boldsymbol{u} + \frac{\bar{\kappa}}{Re}\nabla \cdot \boldsymbol{a}, \tag{24}$$

$$(\partial_t + \boldsymbol{U} \cdot \nabla)\boldsymbol{a} - (\boldsymbol{a} \cdot \nabla \boldsymbol{U} + (\nabla \boldsymbol{U})^T \cdot \boldsymbol{a}) - (\boldsymbol{A} \cdot \nabla \boldsymbol{u} + (\nabla \boldsymbol{u})^T \cdot \boldsymbol{A}) + \frac{1}{De}\boldsymbol{a} = \frac{1}{De}\dot{\gamma}, \tag{25}$$

$$\nabla \cdot \boldsymbol{u} = 0. \tag{26}$$

From the previous section it is known that

$$\boldsymbol{U} = \Omega \cdot \boldsymbol{x}, \qquad \boldsymbol{A} = \frac{\dot{\Gamma}}{1 + 4De^2}\begin{bmatrix} -2E & De \\ 1 & 2De/E \end{bmatrix}. \tag{27}$$

Following Bayly, we seek plane-wave solutions which are a generalization for elliptic flows of the inertial waves in a rigidly rotating fluid. For rigidly rotating flows one can show the existence of plane-wave solutions in a frame rotating with the medium (cf. Greenspan 1968, p. 185), and such waves appear to have a rotating wavevector when viewed in the inertial frame. Bayly (1986) successfully used such normal modes in the elliptic flow, with the constancy of the flow gradients being responsible for the success of the method. Given the similarity of our base state, we look for solutions of the form

$$[\boldsymbol{u}, p, \boldsymbol{a}] = [\boldsymbol{u}'(t), p'(t), \boldsymbol{a}'(t)]\ \mathrm{e}^{\mathrm{i}\boldsymbol{k}(t)\cdot\boldsymbol{x}}. \tag{28}$$

Insertion of the above form into the equations yields (after dropping the primes)

$$\dot{u}_i + \mathrm{i}\dot{k}_m x_m u_i + \mathrm{i}\Omega_{lm} x_m k_l u_i + u_m \Omega_{im} = -\mathrm{i}k_i p - \frac{\kappa}{Re}k^2 u_i + \frac{\mathrm{i}\bar{\kappa}}{Re}k_m a_{mi}, \tag{29}$$

$$\dot{a}_{ij} + \mathrm{i}\dot{k}_m x_m a_{ij} + \mathrm{i}\Omega_{lm} x_m k_l a_{ij} - (a_{im}\Omega_{jm} + \Omega_{im}a_{mj}) - \mathrm{i}(A_{im}k_m u_j + k_m u_i A_{mj}) + \frac{1}{De}a_{ij} = \frac{\mathrm{i}}{De}(k_i u_j + k_j u_i), \tag{30}$$

$$k_m u_m = 0, \tag{31}$$

with the tensor $\Omega_{ij} = E^{-1}\delta_{i2}\delta_{j1} - E\delta_{i1}\delta_{j2}$.

The solution proceeds as follows. First, it is argued that terms proportional to $\boldsymbol{x}$ in both (29) and (30) should cancel. This could be viewed as the *geometric optics*

approximation to the problem, which yields the equation governing the wavevector (the gradient of the eikonal):

$$\dot{k}_m = -k_l \Omega_{lm}. \tag{32}$$

The above equation for $\boldsymbol{k}$, valid in the inviscid case (Bayly 1986), extends to both the Newtonian and viscoelastic cases. In other words, the solution is still in the form of

$$\boldsymbol{k}(t) = [\sin\theta\cos(t - t_o), \quad E\sin\theta\sin(t - t_o), \quad \cos\theta]^T, \tag{33}$$

where the inclination parameter, θ, is the angle of closest approach of the wavevector to the vortex (out-of-plane) axis, and the tip of the wavevector traces an ellipse with the same eccentricity as the streamlines but with the major and minor axes switched (recall wavenumber is reciprocal length). For future reference we provide the expression for k^2 at this point:

$$k^2(t) = \left[1 + (E^2 - 1)\sin^2\theta\sin^2 t\right]. \tag{34}$$

With the wavevector defined as above, the equations simplify so that their coefficients are independent of space, and are periodic in time. The equations read

$$\dot{u}_i + u_m \Omega_{im} = -\mathrm{i}k_i p - \frac{\kappa}{Re}k^2 u_i + \frac{\mathrm{i}\bar{\kappa}}{Re}k_m a_{mi}, \tag{35}$$

$$\dot{a}_{ij} - (a_{im}\Omega_{jm} + \Omega_{im}a_{mj}) - \mathrm{i}(A_{im}u_j + u_i A_{mj})k_m + \frac{1}{De}a_{ij} = \frac{\mathrm{i}}{De}(k_i u_j + k_j u_i), \tag{36}$$

$$k_m u_m = 0. \tag{37}$$

To solve the equations we first eliminate the pressure amplitude, p, by projecting it out of the momentum equation (35). This is done since the flow is incompressible and the waves should be transverse. The projection is achieved by taking the inner product with $(\delta_{ri} - k^{-2}k_r k_i)$. The momentum equation then reads

$$\dot{u}_r - k^{-2}k_r k_i \dot{u}_i + u_m \Omega_{rm} - k^{-2}k_r k_i u_m \Omega_{im} = -\frac{\kappa}{Re}(k^2 u_r - k_r k_i u_i) + \frac{\mathrm{i}\bar{\kappa}}{Re}(\delta_{ri} - k^{-2}k_r k_i)k_m a_{mi}. \tag{38}$$

The above equation is almost in the Floquet form, except that there are two time-differentiated terms. However the time derivative of the continuity equation (31) may be used to replace $k_i \dot{u}_i$ by $-\dot{k}_i u_i$, which can further be simplified to $k_m \Omega_{mi} u_i$ using (32). The final form of the disturbance momentum equation is therefore

$$\dot{u}_r - (2k^{-2}k_r k_i - \delta_{ri})\Omega_{im}u_m = \frac{1}{Re}(\delta_{ri} - k^{-2}k_r k_i)\left[-\kappa k^2 u_i + \bar{\kappa}k_m \tilde{a}_{mi}\right], \tag{39}$$

where, for notational simplification, we have introduced $\mathrm{i}\boldsymbol{a} \equiv \tilde{\boldsymbol{a}}$. The equation for the amplitude of the polymer stress tensor reads

$$\dot{\tilde{a}}_{ij} - (\tilde{a}_{im}\Omega_{jm} + \Omega_{im}\tilde{a}_{mj}) + (A_{im}u_j + u_i A_{mj})k_m + \frac{1}{De}\tilde{a}_{ij} = -\frac{1}{De}(k_i u_j + k_j u_i). \tag{40}$$

Noting the time-periodic nature of $\boldsymbol{k}$, the above equations are a Floquet system for the nine unknowns: $\boldsymbol{u}$ and the symmetric part of $\tilde{\boldsymbol{a}}$. The problem is then of the general form

$$\dot{\boldsymbol{X}} + \boldsymbol{C}(t)\cdot\boldsymbol{X} = 0, \qquad \boldsymbol{X} \equiv [u_1, u_2, u_3, \tilde{a}_{11}, \tilde{a}_{22}, \tilde{a}_{33}, \tilde{a}_{12}, \tilde{a}_{13}, \tilde{a}_{23}]^T, \tag{41}$$

for some periodic $\boldsymbol{C}(t)$ with period $T = 2\pi$. We term matrix $\boldsymbol{C}$ the Floquet matrix, the entries of which are given in the Appendix. The solution is then of the form (cf.

Grimshaw 1990)

$$\boldsymbol{X}(t) = \mathrm{e}^{\sigma t}\bar{\boldsymbol{X}}(t), \tag{42}$$

where $\bar{\boldsymbol{X}}$ is periodic in its argument with period 2π. Stability of the problem is determined by the Floquet exponent, σ. This exponent is related to the eigenvalues μ of the fundamental matrix of (41), $\boldsymbol{M}(2\pi)$, corresponding to the initial condition $\boldsymbol{M}(0) = \boldsymbol{I}$ as follows:

$$\mathrm{e}^{2\pi\sigma} = \mu. \tag{43}$$

The vectors $\bar{\boldsymbol{X}}$ are the corresponding eigenvectors. The fundamental matrix satisfies the same equation as (41):

$$\dot{\boldsymbol{M}} + \boldsymbol{C}(t)\cdot\boldsymbol{M} = 0. \tag{44}$$

5. Results

In this section we present results from a comprehensive set of studies of the instability of the elliptic-streamline flow. The results are ordered so as to put the present study in the proper context. Thus we first recapitulate the relevant parameters of the problem and the parametric dependencies of the basic-state flow and stresses, as well as of the disturbances to the same. Next, the inviscid results of Bayly (1986) are reproduced in order to provide a basis of comparison for the viscous and the viscoelastic results which follow. Bayly (1986) and Pierrehumbert (1986) focused solely on the inviscid dynamics as it was deemed (rightly so) that (Newtonian) viscous effects will merely modify the nature of the instabilities and not give rise to new phenomena. This is a valid conclusion based on the observation of the time scale of the evolution of the instabilities, which is clearly inertial. However, the neglect of molecular viscosity will introduce anomalies such as the lack of any cutoff in wavenumber space for the unstable modes. Intuitively one would expect there to be a cutoff once the wavelength becomes small enough that the Reynolds number based on the wavelength is no longer very large.

In order to investigate the effect of viscoelasticity on the stability characteristics of the elliptic flow, one should first include the Newtonian viscous effects in the analysis of Bayly. Otherwise any prediction of cutoffs or stabilization might be taken out of context and one might incorrectly attribute the changes to viscoelasticity rather than to molecular viscosity. Accordingly, effects of Newtonian (molecular) viscosity are investigated by a simple extension of Bayly's analysis, with the inclusion of viscosity stabilizing the flow exactly as one would have guessed: at each eccentricity, E, both the maximum growth rate and the range of unstable inclination angles, θ, are reduced.

Finally the effects of polymer stresses on the instability of the elliptic flow are presented. These results – and the discussion of their mathematical and physical underpinnings – are the main contributions of the present work. It is shown that unlike their Newtonian counterpart, the polymer stresses are capable of giving rise to *new* secular instabilities, thereby enlarging the unstable volume in the parameter space. Our results indicate that for larger eccentricities some wavevectors which were inviscidly stable become unstable. These wavevectors are almost normal to the 3-direction, i.e. these are waves which propagate nearly in the plane of the base flow. The mathematical and physical nature of the latter instabilities are investigated in the discussion section aided by the development of a model oscillator equation.

5.1. *Recapitulation of the governing parameters*

Before embarking on the presentation of results, let us recapitulate the parametric dependencies of various basic-state and disturbance quantities.

5.1.1. *Basic-state velocity:* $\boldsymbol{U} = \boldsymbol{U}(E)$

The linear basic-state velocity field depends only on the eccentricity parameter E. The Reynolds number does not appear owing to the linearity of the flow. Moreover, as was shown, the polymer stress field is a constant tensor which makes no contribution to the dynamics of the basic state. The geometric parameter is a measure of the amount of strain in the base state.

5.1.2. *Basic-state polymer stress:* $\boldsymbol{A} = \boldsymbol{A}(E, De)$

The dependence of the normal polymer stresses on De is of the form $De/(1 + De^2)$, which is the hallmark of viscoelastic behaviour in a time-periodic flow (cf. Bird *et al.* 1987). The polymer is inactive as $De \to 0$ (infinitely fast relaxation), and it is purely elastic as $De \to \infty$. The parametric dependence of the base state exposes the simple fact that polymer effects are strongest where the time scale of the flow is comparable to the relaxation scale of the polymer. We comment however that, in contrast to Eulerian time-periodic flows, elastic stresses can survive in the limit $De \to \infty$ if $E \gg 1$, as can be seen from (22). As $E \to \infty$, the flow approaches a parallel shear flow which can support large streamwise polymer stretch, as discussed by Azaiez & Homsy (1994*a*).

5.1.3. *Linear disturbances:* $q(\boldsymbol{x}, t) = q'(t) \exp\{\mathrm{i}\boldsymbol{k}(t) \cdot \boldsymbol{x}\}$

In the above expression q denotes the disturbance to the generic basic-state variable Q. The wavevector $\boldsymbol{k}(t)$ is characterized by the inclination angle θ, and the magnitude, k_o, the latter giving the length scale used to define the Reynolds number.

The limit $E \to \infty$ in the elliptic flow promotes polymer effects on the disturbance dynamics in the elastic limit $De \to \infty$ as well. This is best seen from the behaviour of the normal excess stresses in (22), where a sufficiently large $E(\sim ReDe)$ can be found which results in non-negligible contributions by the polymers to the disturbance dynamics.

The (complex) maximum growth rate, σ, of the instability is a function of all the parameters of the problem:

$$\sigma = \sigma(E, Re, De, \theta, \kappa). \tag{45}$$

By making assumptions, such as an inviscid or Newtonian flow ($Re \to \infty, De = 0$ respectively), one can simplify the parametric dependence of the growth rate. These assumptions will be relaxed one at a time in order to recover the complete parametric dependence.

5.2. *Inviscid instability*

By neglecting the excess stresses, the governing equations for the disturbances reduce to those of Bayly's (1986) study. The growth rate has the following simplified parametric dependence:

$$\sigma = \sigma(E, \theta). \tag{46}$$

Bayly argued that for high enough wavenumbers the disturbances become self-similar, with the wavenumber measure k_o disappearing from the final results. The results of Bayly are recalculated and presented in figure 1 as contours of the growth rate in the (θ, E)-plane. Several points need to be noted. First, for $E = 1$, corresponding to a rigidly rotating circular flow, all disturbances are neutrally stable, a well-known property of inertial waves in rotating systems (cf. Greenspan 1968, p. 185). Second, for $E > 1$ there exists a band of orientations of the wavenumbers that experience a secular instability on the inertial time scale. The mechanism is that

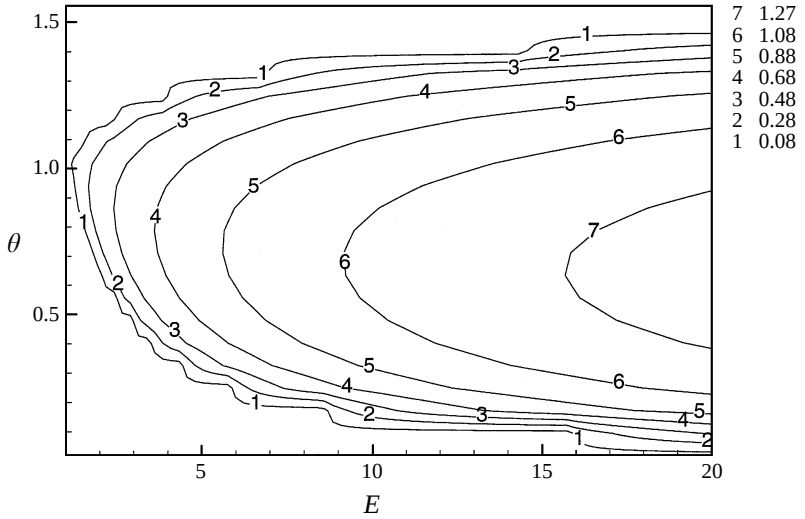

FIGURE 1. Stability diagram: inviscid case.

of the tilting and stretching of vortices, which is operative only in three-dimensional flows. So while the base flow is two-dimensional, it is essential for instability that the disturbances be three-dimensional. This point is further noted by observing that there are no instabilities on the line $\theta = \pi/2$ corresponding to two-dimensional modes. This point is extremely important; the reader should compare this observation to the new viscoelastic modes discussed later in this section.

The region outside of the band of instabilities is neutrally stable. As noted by Bayly (1986) the neutral instability is a consequence of the traceless nature (over one period) of the Floquet matrix – the appropriately reduced version of $\boldsymbol{C}$ from (44) – which guarantees the determinant of $\boldsymbol{M}(2\pi)$ to be unity. Furthermore, the form of the equations shows that

$$\frac{\mathrm{d}}{\mathrm{d}t}(\boldsymbol{k}\cdot\boldsymbol{M}) = 0, \tag{47}$$

which implies that

$$\boldsymbol{k}(0) = \boldsymbol{k}(2\pi)\cdot\boldsymbol{M}(2\pi) = \boldsymbol{k}(0)\cdot\boldsymbol{M}(2\pi), \tag{48}$$

so that one eigenvalue is always unity. The other two are either real and the reciprocal of one another (unstable case), or are a complex-conjugate pair on the unit circle (neutrally stable case).

5.3. *Viscous instability: Newtonian*

An anomalous conclusion from the inviscid analysis is the absence of any high-wavenumber cutoff of the instability. In other words, the self-similarity of the inviscid instability implies the possibility of a 'bottomless' cascade. However, experience dictates the existence of a cutoff in wavenumber space, beyond which the instability is moderated owing to viscous dissipation. This constitutes a simple but useful extension of Bayly's analysis. Therefore we set $De = 0$, $\kappa = 1$ in (44), thus reducing the problem to its Newtonian limit. The stability analysis results in a growth rate

$$\sigma = \sigma(E, \theta, Re), \tag{49}$$

which clearly indicates the dependence of the instability on the length scale, as captured by Re. The Floquet equation governing the evolution of the fundamental matrix in the present case is

$$\frac{\mathrm{d}}{\mathrm{d}t}\boldsymbol{M} = \left(2\frac{\boldsymbol{kk}}{k^2} - \boldsymbol{I}\right) \cdot \Omega \cdot \boldsymbol{M} - \frac{k^2}{Re}\boldsymbol{M}. \tag{50}$$

Taking the inner product with $\boldsymbol{k}$ and performing some algebraic simplifications one obtains

$$\frac{\mathrm{d}}{\mathrm{d}t}(\boldsymbol{k}\cdot\boldsymbol{M}) + \frac{k^2}{Re}\boldsymbol{k}\cdot\boldsymbol{M} = 0, \tag{51}$$

which has the following solution:

$$[\boldsymbol{k}\cdot\boldsymbol{M}](t) = [\boldsymbol{k}\cdot\boldsymbol{M}](0)\exp\left\{-\int_0^t \frac{k^2}{Re}\,\mathrm{d}t\right\}. \tag{52}$$

Using the periodic nature of $\boldsymbol{k}$ we obtain

$$\boldsymbol{k}(0)\cdot\boldsymbol{M}(2\pi) = \boldsymbol{k}(0)\exp\left\{-\frac{2\pi}{Re}\left[1 + \frac{E^2-1}{2}\sin^2\theta\right]\right\}, \tag{53}$$

so that the growth rate is $-(1 + \frac{1}{2}(E^2-1)\sin^2\theta)/Re$. Outside the band of instability in θ there now exists an asymptotically stable region with a decay rate proportional to the Newtonian viscosity, and inversely proportional to the square of the scale of the disturbance.

We find that the inertial instabilities studied by Bayly (1986) are moderated upon the introduction of Newtonian viscosity, more so as their scales become smaller. The stability diagrams are given in figure 2(*a*)–2(*c*) for three values of Re. As expected, results for increasing values of Re simply trend towards those for $Re \to \infty$ shown in figure 1. The viscous results show a reduction in the extent of the zone of instability, a reduction in the maximum growth rate, and a decay outside the zone of instability where previously there were neutrally stable waves. The decay rate is larger for larger values of θ, i.e. for waves whose wavenumber lies closer to the plane of the base flow. For the same magnitude of wavenumber, the larger θ implies a smaller minimum scale in each period of rotation – obtained when the projection of $\boldsymbol{k}$ on the plane of the flow points along the minor axis of the base elliptic flow – than that for a wavenumber having a smaller inclination. The larger the inclination, the larger the projection of a given wavenumber on the plane of the flow, the smaller the resulting scales, and the more effective the viscous dissipation.

5.4. *Viscous instability: non-Newtonian*

We find that considering the complete 9×9 system in (41) results in a dramatically different stability diagram. In order to focus on viscoelastic effects, we set $\kappa = 0$, thus neglecting the Newtonian viscous effects but retaining the Newtonian limit of the polymer stress. The growth rates have a four-parameter dependence:

$$\sigma = \sigma(E, \theta, Re, De). \tag{54}$$

The time-periodic nature of the base flow gives rise to a Deborah-number dependence of the form (neglecting $O(1)$ numerical constants)

$$\frac{De}{1 + De^2}. \tag{55}$$

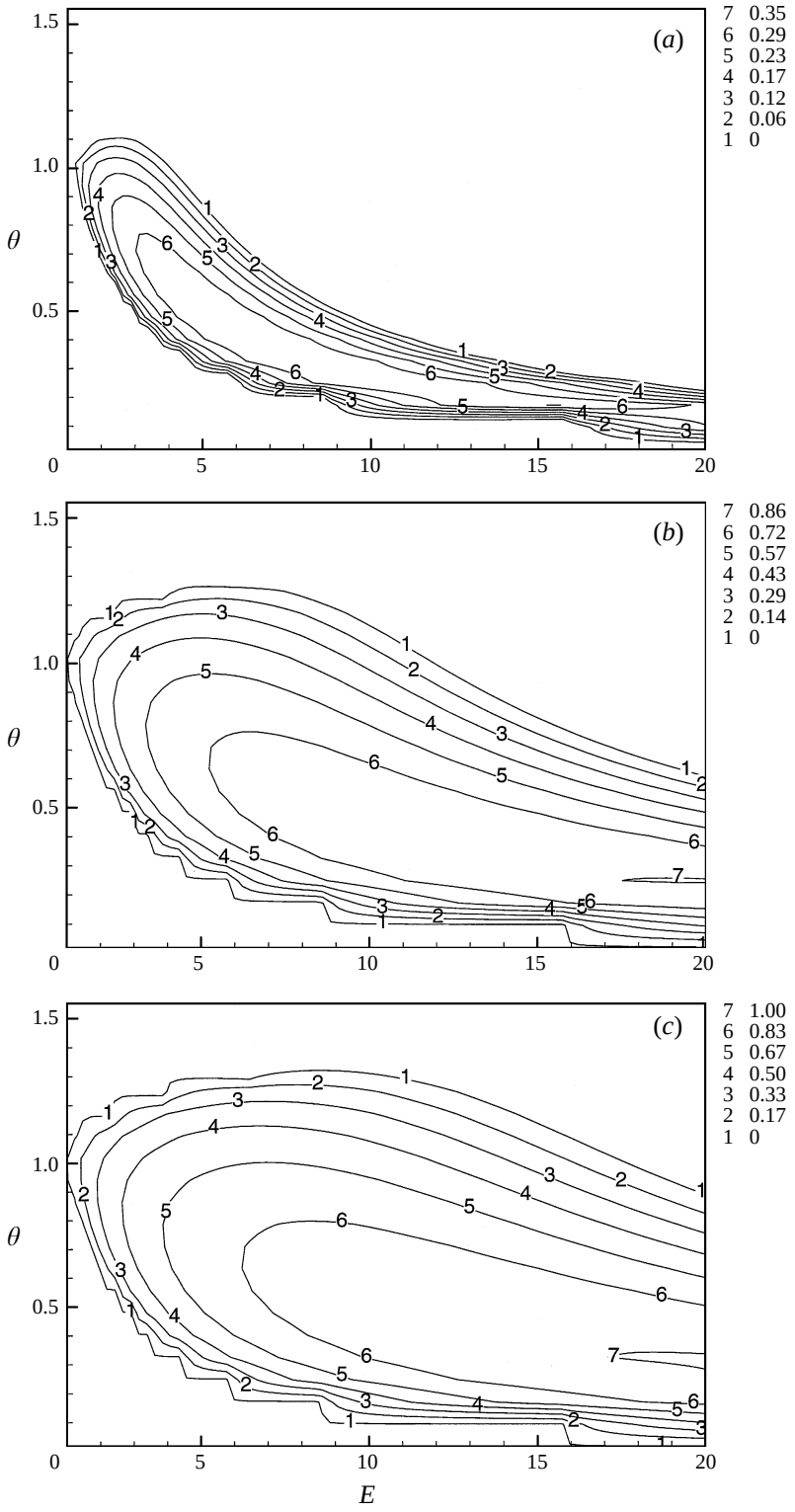

FIGURE 2. Stability diagram: Newtonian viscosity only: (*a*) $Re = 10$, (*b*) $Re = 50$, (*c*) $Re = 100$.

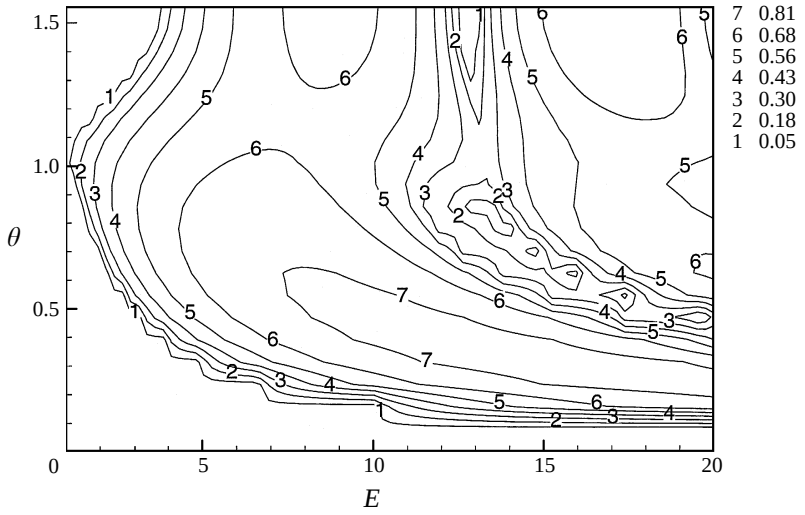

FIGURE 3. Stability diagram: viscoelastic case ($De = 3$, $Re = 9$).

Therefore, assuming $E \sim O(1)$, and referring to (29) and (30) it is apparent that the dynamical effects of the polymer stresses will be strongest when $Re, De \sim O(1)$.

We begin our discussion of the viscoelastic results by adopting the following values for the parameters:

$$De = 3, \qquad Re = 9. \tag{56}$$

These values are both $O(1)$ and result in typical stability diagrams whose features we shall discuss below. At the end of this section we will provide neutral stability diagrams corresponding to a more comprehensive range of parameters.

Figure 3 shows the stability diagram, which exhibits some remarkable features. Most prominent is the extension of the zone of instability to $\theta = \pi/2$, indicating a *new mode of instability wave* propagating in the plane of the flow. (Recall that the inertial mechanism of instability cannot be sustained near $\theta = \pi/2$ as the vortex tilting and stretching mechanisms are turned off in that vicinity.) The mechanism for this new instability is identified and discussed in detail in the next section. A second interesting feature of the stability diagram is the appearance of a ridge pattern throughout. Finally, the lower part of the diagram still resembles its inertial counterpart. All these features will be discussed in detail, and their mathematical and physical origins will be identified. The new modes propagate in or near the plane of the flow; they are longer in the axial direction than they are in the plane of the flow. This is in contrast to the purely inertial instabilities which have a uniform (short) scale in all directions.

A comprehensive parametric study was conducted and the general features of figure 3 were found to be robust as Re and De were varied. Comparing figures 2(a) and 3, it is clear that for fixed Re, there is a critical value of De for which the neutral curve grazes $\theta = \pi/2$ at a particular value of E. Given that the new modes are dominant close to $\theta = \pi/2$, we fix the value of θ at $\pi/2$ and plot the neutral stability curves in the (De, Re)-plane for various values of the eccentricity parameter E, as shown in figure 4.

The most striking feature of the curves is their hyperbolic form. As will be discussed below, this hyperbolicity results from the instability condition that

$$\frac{(E^2 - 1)De}{(1 + 4De^2)Re} \geqslant 1 \tag{57}$$

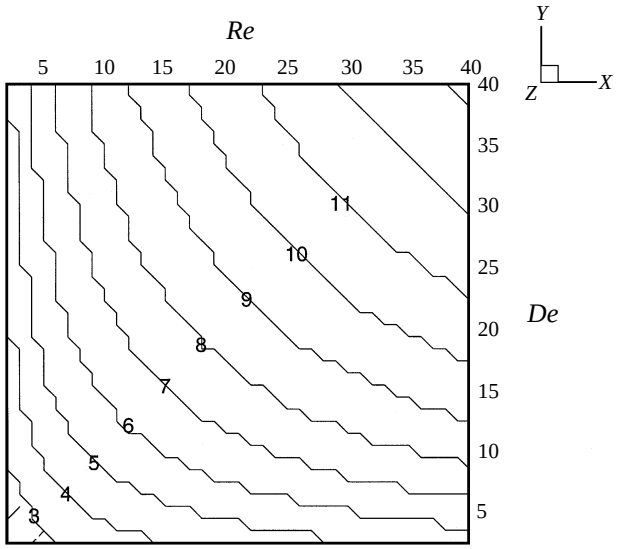

FIGURE 4. Neutral-stability diagrams for various values of the eccentricity, E (denoted on each curve). The region below each curve corresponds to stability.

with the neutral stability corresponding to equality. Thus the neutral curves, parametrized by E, are hyperbolae for modest to large values of De.

Physically, figure 4 states that for any given flow ($E \sim O(1)$) and $Re \sim O(1)$, the contributions of the polymer to the dynamics are felt and can give rise to instabilities if the relaxation time scale of the polymer is close to the period of the flow, i.e. there is a finite, continuous interval of instability in De. As the flow becomes more viscous, a larger range of polymer relaxation time scales are capable of coupling to the dynamics of the flow, and the excess stresses are promoted through the enhancement of the polymer viscosity. However, this observation needs to be qualified because the stability diagram was constructed while neglecting Newtonian viscosity. As $Re \to 0$ the Newtonian viscosity will damp the instabilities and will in all likelihood make the axis $Re = 0$ a stable zone. This conjecture could be checked by allowing for a non-zero value of κ. While not difficult to analyse, the effect of finite κ can be easily anticipated from figure 2(a) of §5.3 to be a general damping and narrowing of the band of unstable modes.

For any prescribed E there exists a Re and De above which the flow is stable. The stabilization for each parameter occurs for different reasons as follows. As Re becomes sufficiently large (at fixed E), the polymer viscosity becomes small (or equivalently the wavelength becomes large) so that the polymers produce an extra stress driven by the flow but are unable to couple back to the dynamics of the flow. Conversely, as De becomes large, the relaxation time scale of the polymer becomes so disparate from the period of the flow that only small polymeric stresses can be produced and again there is a dynamical decoupling.

In order to point out the effects of the polymers in the limits of zero or infinite De, we perform a simple scale analysis of the evolution equation for the linear disturbances, $\boldsymbol{a}$, to the polymer base-state stress, $\boldsymbol{A}$:

$$\dot{\boldsymbol{a}} - (\boldsymbol{a}\cdot\nabla\boldsymbol{U} + (\nabla\boldsymbol{U})^T\cdot\boldsymbol{a}) - (\boldsymbol{A}\cdot\nabla\boldsymbol{u} + (\nabla\boldsymbol{u})^T\cdot\boldsymbol{A}) + \frac{1}{De}\boldsymbol{a} = \frac{1}{De}\dot{\boldsymbol{\gamma}}, \tag{58}$$

where the time derivative is taken moving with the base flow.

$De \to 0$: There is instant relaxation of stresses and perfect phase matching between the polymer stress and the flow strain rate. Therefore, the result is a modified Newtonian viscosity. This is seen from (58) which in the above limit is

$$a \approx ku \approx u \quad [k = O(1)], \tag{59}$$

and in the momentum equation both the polymer stress and the Newtonian viscous stress are of the order of

$$\frac{k^2}{Re} u \left(\approx \frac{1}{Re} u \right). \tag{60}$$

In this limit the polymer stress will simply modify the viscosity. The effect is felt for Reynolds numbers which are small to moderate, i.e. at scales of the order of the viscous diffusion length.

$De \to \infty$: There is no relaxation and the polymers are perfectly elastic. From (21) the term (in (58)) involving the basic-state tensor, $\boldsymbol{A}$, is implicitly $O(De^{-1})$ (assuming E is $O(1)$). There are two other terms in the equation which are explicitly $O(De^{-1})$. Thus in the limit of large De, the strain rate of the polymer is being forced by terms which are $O(De^{-1})$, so that at steady state one has

$$a \approx \frac{u}{De}.$$

In the momentum equation then the viscous terms are of the following orders:

$$\text{Newtonian: } \frac{u}{Re}, \quad \text{polymer: } \frac{u}{De\ Re},$$

so that the polymer stress is of a much smaller order than the Newtonian one and the non-Newtonian effects are essentially absent.

A somewhat subtle point needs to be reiterated. The actual parametric dependence of the components of the base-state strain rate, in the limit of large E and De, is $O(E^2 De^{-1})$. Therefore the non-Newtonian effects can be felt, even for large De, so long as

$$E^2 \sim DeRe. \tag{61}$$

In this limit the extreme ellipticity supports polymer stresses in a fashion analogous to a parallel shear flow. As discussed by Azaiez & Homsy 1994(*a*), elastic effects are then possible for high Re, De in the distinguished limit $De/Re \sim O(1)$ in the sense of intermediate asymptotics, as the constitutive equation must also be 'Oldroyd-B like' over some range of Re and De. We do not pursue this issue here.

The above conclusions apply to the polymer-dominated case for modes corresponding to $\theta = \pi/2$. But we comment that for some combination of parameters (E, Re, De) there may be purely inertial instability modes for oblique waves which have comparable or greater growth rates than the viscoelastic instability modes under study, giving rise to mode competitions and multi-mode instabilities.

6. Mechanism of the new instability

In this section we study the physical mechanism responsible for the new instability modes discussed in the previous section. The first phase of the investigation is mathematical. A thorough term-by-term interrogation of the full governing equations is conducted in order to identify the terms responsible for the new instability. The second phase uses the insight so generated to simplify the equations by first stripping them of the non-essential terms and then reducing them to a single model equation

of Mathieu form. All the features of the stability diagrams of the full problem are then inferred from this Mathieu equation and its well-known stability diagram. The *quantitative* accuracy of the Mathieu equation then allows a physical description of the mechanism of instability.

6.1. *Term-by-term interrogation*

In order to determine the role of each term of (25) on the observed instability, we modify the equation by introducing 'switches' s_i which are either 1 or 0, and are used to turn various terms on or off:

$$\dot{\boldsymbol{a}} - s_1(\boldsymbol{a}\cdot\nabla\boldsymbol{U} + (\nabla\boldsymbol{U})^T\cdot\boldsymbol{a}) - s_2(\boldsymbol{A}\cdot\nabla\boldsymbol{u} + (\nabla\boldsymbol{u})^T\cdot\boldsymbol{A}) + \frac{1}{De}\boldsymbol{a} - \frac{s_3}{De}\dot{\boldsymbol{\gamma}} = 0. \tag{62}$$

s_1 is associated with the production of perturbation stress through the base-state velocity gradient; s_2, that due to the coupling of the perturbation velocity with the base-state stress; and s_3 the viscous relaxation of perturbation stress. In figures 3, 5(*a–f*) we present the stability diagram obtained for each of the seven non-trivial permutations of the three switches for the case $Re = 9$, $De = 3$, and $\kappa = 0$. Figure 3 is the base-line stability diagram corresponding to all three switches being turned on. Figures 5(*a*), 5(*b*), and 5(*c*) correspond to only one of the three switches being turned on, while the remaining three figures correspond to pairwise activation of the switches. The results in figure 5(*a*) show clearly that the interactions of the gradients of the base flow with the polymer disturbance, $(s_1, s_2, s_3) = (1, 0, 0)$, have no stability ramifications. They are neither stabilizing nor destabilizing, as evidenced by the fact that the stability diagram is both qualitatively and quantitatively the same as its inviscid counterpart (figure 1). Because of this we refer to this term as a redistribution term: it merely redistributes the polymer stresses by moving them around according to the base-state flow, but it does not generate or relieve stresses. The interactions of the base-state stresses and the gradients of the disturbance velocity – $(s_1, s_2, s_3) = (0, 1, 0)$ – are found to be the main contributors to the new instability mechanism being discussed. These terms give rise to the enlargement of the unstable zone, as well as the instability of waves propagating in the plane of the flow. Finally, the terms resulting from the viscous response of the disturbances – $(s_1, s_2, s_3) = (0, 0, 1)$ – are seen to make an interesting contribution to the instability mechanism at hand. The shear terms give rise to well-defined striations and ridge patterns on the stability diagram. Therefore the term of highest dynamical significance in producing the new instability is that of the interaction of the base-state polymer stress with the gradients of the velocity perturbations. The next significant term is the contribution of a viscous component to the polymer stress due to the shear of the disturbances. Figures 5(*d*)–5(*f*) show the stability diagrams for the pairwise activation of the switches. It is clear that the universal features of the diagrams above are retained.

6.2. *The oscillator model equation*

Having investigated the dynamic relevance of the terms in (24) and (25), we study the behaviour of the following model equations which contain only the dynamically relevant terms for the polymer-induced instability:

$$\dot{\boldsymbol{u}}' = -\nabla p' + \frac{1}{Re}\nabla\cdot\boldsymbol{a}', \tag{63}$$

$$\dot{\boldsymbol{a}}' + \frac{1}{De}\boldsymbol{a}' = \alpha\left[\boldsymbol{A}\cdot\nabla\boldsymbol{u}' + (\nabla\boldsymbol{u}')^T\cdot\boldsymbol{A}\right] + \frac{\beta}{De}\left[\nabla\boldsymbol{u}' + (\nabla\boldsymbol{u}')^T\right], \tag{64}$$

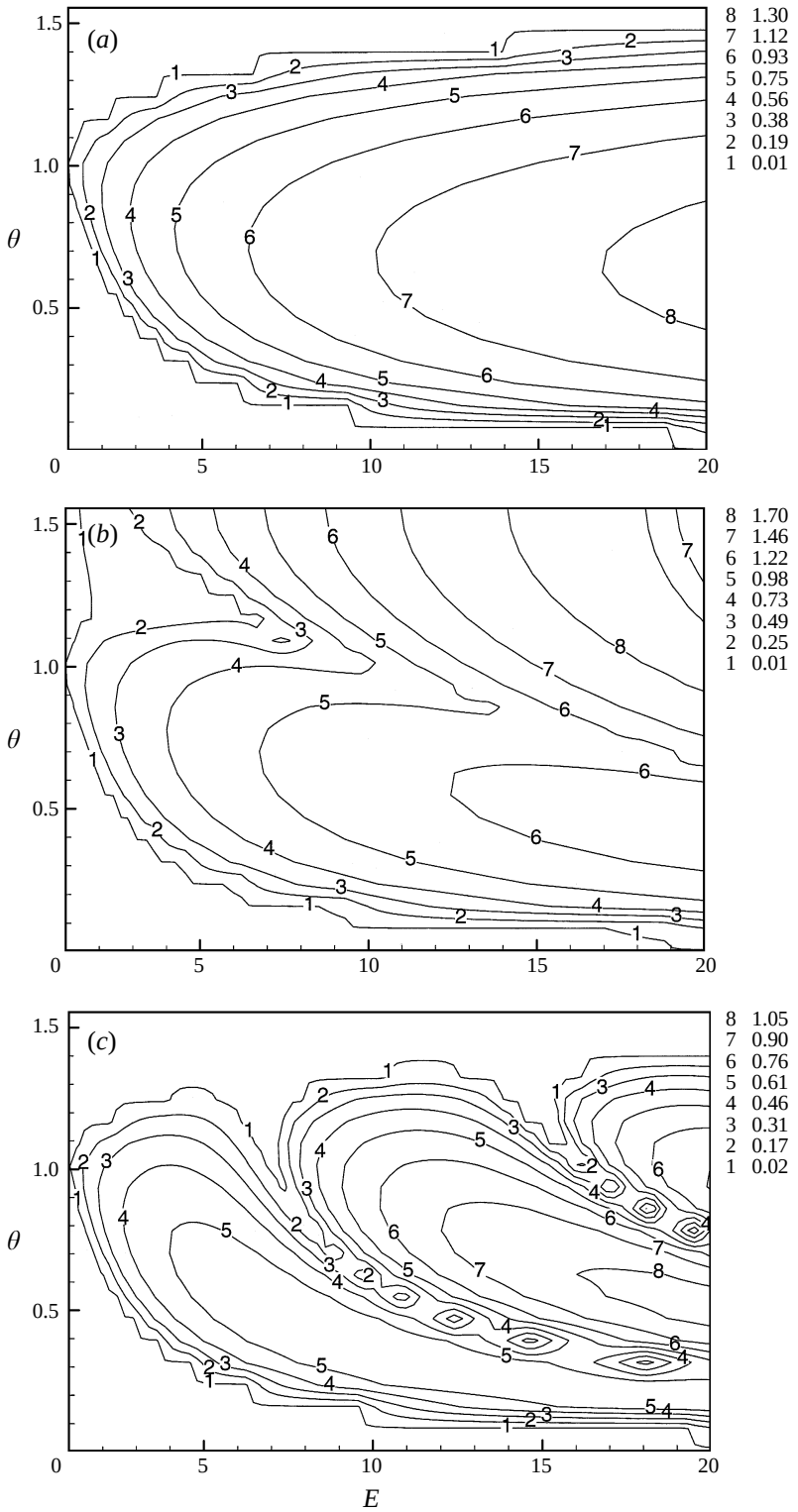

FIGURE 5. (*a*)–(*c*) For caption see facing page.

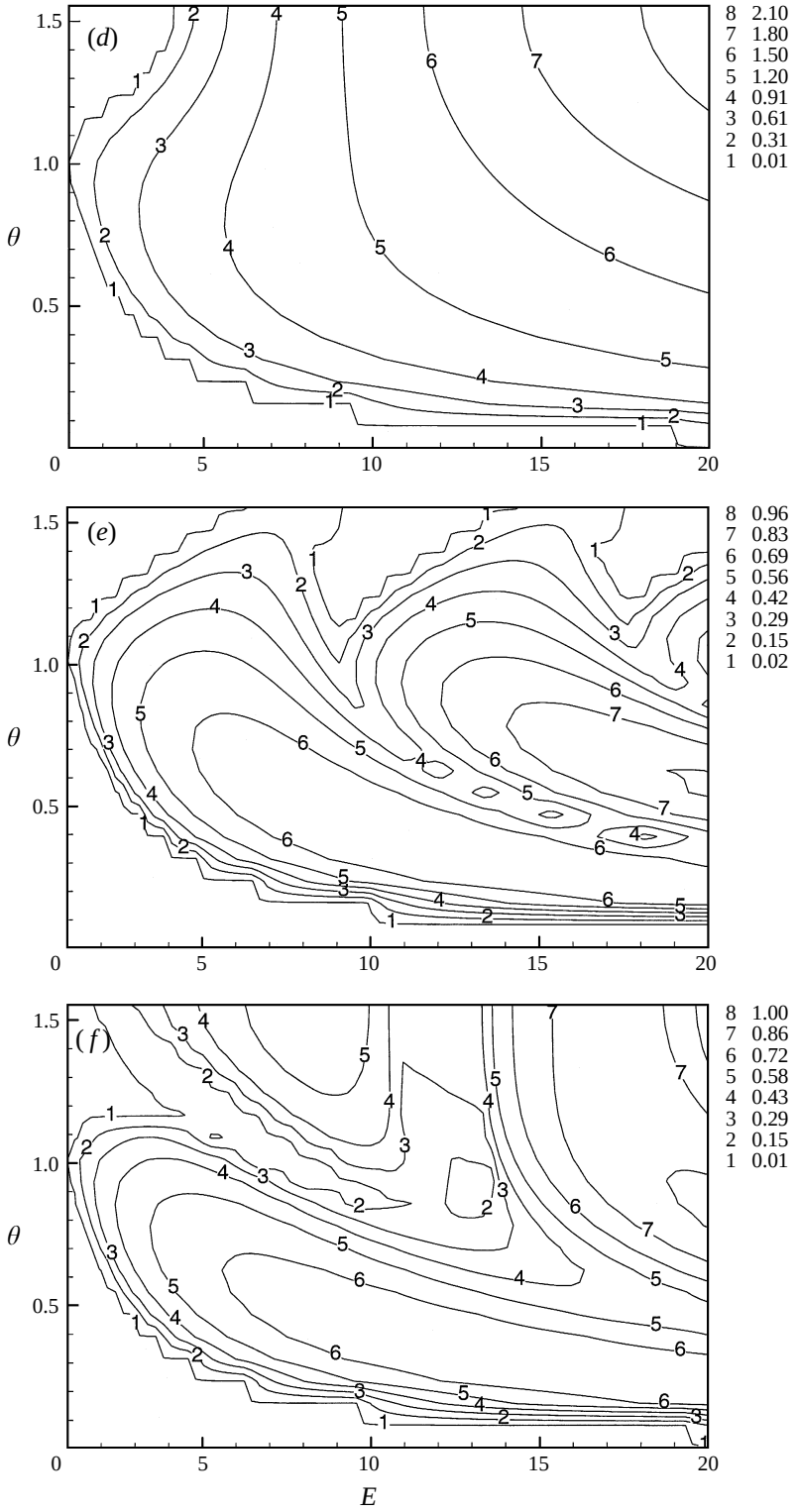

FIGURE 5. Stability diagram for the term-by-term interrogation of the equations: 'swith' analysis of (62) with (*a*) $(s_1, s_2, s_3) = (1, 0, 0)$, (*b*) $(s_1, s_2, s_3) = (0, 1, 0)$, (*c*) $(s_1, s_2, s_3) = (0, 0, 1)$, (*d*) $(s_1, s_2, s_3) = (1, 1, 0)$, (*e*) $(s_1, s_2, s_3) = (1, 0, 1)$, (*f*) $(s_1, s_2, s_3) = (0, 1, 1)$.

where $\boldsymbol{u}'$ and $\boldsymbol{a}'$ are the total disturbances to the corresponding base-state quantities rather than the wave amplitudes. The multipliers α and β will be used to tag and distinguish the contribution of the disturbance shear from that of the base-state stress. All the convective redistribution terms and the Newtonian viscous terms have been neglected. Performing the following manipulation:

$$\left(\nabla \wedge + \frac{1}{De}\right) \times \text{equation (63)},$$

and using (64) to eliminate the time derivative of $\boldsymbol{a}'$, one obtains the following (vector) equation for the disturbance vorticity $\boldsymbol{\zeta}'(\equiv \nabla \wedge \boldsymbol{u}')$:

$$\ddot{\boldsymbol{\zeta}}' + \frac{1}{De}\dot{\boldsymbol{\zeta}}' = \frac{1}{Re}\nabla \wedge \left[\alpha \nabla \cdot \left(\boldsymbol{A} \cdot \nabla \boldsymbol{u} + (\nabla \boldsymbol{u})^T \cdot \boldsymbol{A}\right) + \beta \frac{\nabla^2 \boldsymbol{u}}{De}\right]. \tag{65}$$

Using the continuity equation for $\boldsymbol{u}'$ and the fact that $\boldsymbol{A}$ is spatially constant, the above equation can be simplified:

$$\ddot{\boldsymbol{\zeta}}' + \frac{1}{De}\dot{\boldsymbol{\zeta}}' = \frac{1}{Re}\left[\alpha \boldsymbol{A} : \nabla\nabla\boldsymbol{\zeta}' + \beta \frac{\nabla^2 \boldsymbol{\zeta}'}{De}\right]. \tag{66}$$

Next, we note that the disturbance vorticity has the same normal-mode form as the other disturbances:

$$\boldsymbol{\zeta}'(\boldsymbol{x}, t) = \boldsymbol{\zeta}(t) \exp[\mathrm{i}(\boldsymbol{k}(t) \cdot \boldsymbol{x})]. \tag{67}$$

At this point a further simplifying assumption is made in order to arrive at a model oscillator equation. We ignore the contributions of the time variations of the wavenumber to the time variations of $\boldsymbol{\zeta}'$. If one were to differentiate both sides of (67), there would be a large number of terms involving the time derivatives of $\boldsymbol{k}$, which we argue are of secondary importance. The only aspect of $\boldsymbol{k}$ which is important for polymeric instability is its rotation. The fact that there are slight variations in its rate of rotation is not of dynamical significance. Therefore one obtains the simple equation

$$\ddot{\boldsymbol{\zeta}} + \frac{1}{De}\dot{\boldsymbol{\zeta}} = -\frac{1}{Re}\left[\alpha(\boldsymbol{k} \cdot \boldsymbol{A} \cdot \boldsymbol{k}) + \beta \frac{k^2}{De}\right] \boldsymbol{\zeta}. \tag{68}$$

Furthermore, it is noted that the coefficients of the above equation are scalars; therefore, the stability characteristics of the underlying operator can be surmised by studying the corresponding scalar equation

$$\ddot{\zeta} + \frac{1}{De}\dot{\zeta} = -\frac{1}{Re}\left[\alpha(\boldsymbol{k} \cdot \boldsymbol{A} \cdot \boldsymbol{k}) + \beta \frac{k^2}{De}\right] \zeta. \tag{69}$$

Using the expressions from (33) and (34) for $\boldsymbol{k}$ and k^2 respectively, the final model oscillator equation reads

$$\ddot{\zeta} + \frac{1}{De}\dot{\zeta} = \alpha \frac{1}{Re} \frac{(E^2 - 1)\sin^2\theta}{1 + 4De^2} (\sin 2t - 2De \cos 2t)\, \zeta - \beta \frac{1}{ReDe}\left[\left(1 + \frac{E^2 - 1}{2}\sin^2\theta\right) - \frac{E^2 - 1}{2}\sin^2\theta \cos 2t\right] \zeta. \tag{70}$$

We now proceed to analyse this equation, which is a Mathieu equation of the form

$$\ddot{\zeta} + \frac{1}{De}\dot{\zeta} = f(2t)\zeta, \tag{71}$$

for a periodic function f.

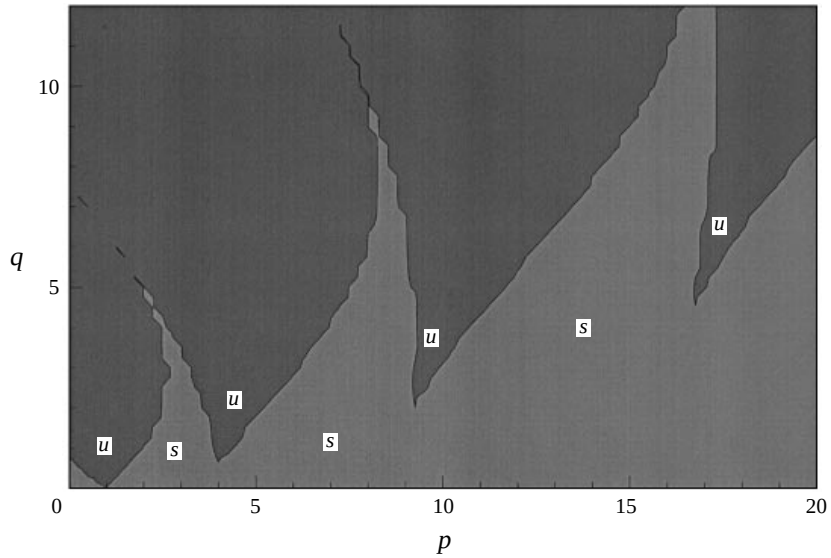

FIGURE 6. Stability diagram: Mathieu equation: *s* denotes stable, *u* unstable.

The generic form of the Mathieu equation is

$$\ddot{u} + (p - 2q\cos 2t)u = 0. \tag{72}$$

The stability diagram (in the p, q plane) for this equation can be obtained using Floquet analysis, and has been studied extensively (e.g. Grimshaw 1990). This diagram is provided in figure 6, and will be used to extract information from (70).

Using the Mathieu diagram (figure 6) we can easily identify the role of the two terms in (69) and (70) producing the features of the stability plots shown in figure 3 by setting α, β to zero, respectively.

$\alpha = 0, \beta = 1$: For one-to-one correspondence of terms between (70) and (72) we find

$$p = \frac{1}{ReDe}\left[1 + \frac{E^2 - 1}{2}\sin^2\theta\right], \qquad q = \frac{1}{4ReDe}\left(E^2 - 1\right)\sin^2\theta. \tag{73}$$

At a fixed θ, as E increases from unity we move along a *ray* in the (p, q)-Mathieu diagram. For E near unity the ray resides solely in the stable regions. As $E^2 - 1$ becomes large, we then cross through regions of stability and instability in the Mathieu diagram. Passage through the unstable zones can somewhat extend the inertially unstable range, while passage through the stable zones can stabilize some of the inertial instabilities. Those features are reflected in the horns and striations for the full problem shown in figure 5(*c*).

$\alpha = 1, \beta = 0$: We rewrite (70) in the form

$$\ddot{\zeta} + \frac{1}{De}\dot{\zeta} = \frac{1}{Re}\left[\frac{(E^2 - 1)\sin^2\theta}{(1 + 4De^2)^{1/2}}\sin[2t - \tan^{-1}(2De)]\right]\zeta. \tag{74}$$

Thus for one-to-one correspondence with (72) one finds

$$p = 0, \qquad q = \frac{1}{Re}\frac{(E^2 - 1)\sin^2\theta}{(1 + 4De^2)^{1/2}}. \tag{75}$$

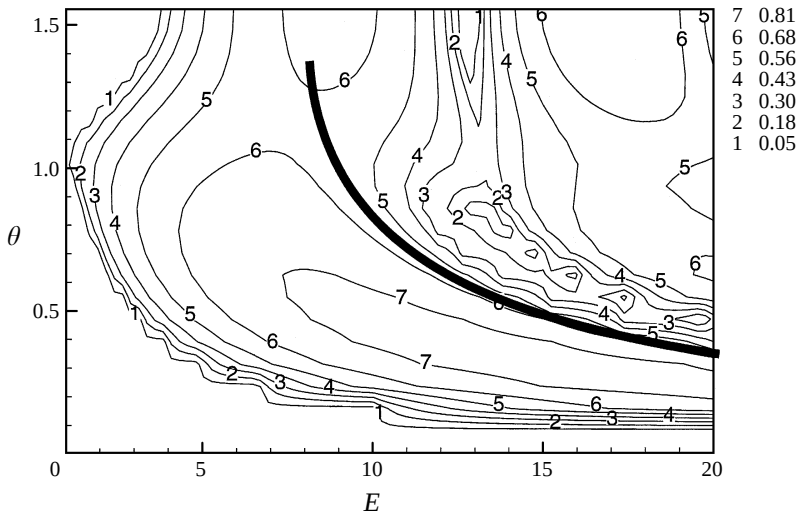

FIGURE 7. Viscoelastic neutral stability curve (equation (76)) superimposed on the stability diagram for $Re = 9$ and $De = 3$.

However from the Mathieu diagram figure 6 it is seen that at $p = 0$ any $q > 1$ gives rise to a secular instability. Therefore the condition for instability is

$$\frac{1}{Re}\frac{(E^2-1)\sin^2\theta}{(1+4De^2)^{1/2}} \geqslant 1, \tag{76}$$

with the neutral curve being given by the equality. This is a remarkably simple and accurate stability criterion. Indeed in figure 7 we have reproduced figure 5(*b*) and added the neutral condition from (76), which tracks almost perfectly the 'canyon' in the figure. The canyon falls between the old zone of inertial instability – which is always present in our results – and the new zone created by the effect of the polymers. The line which is drawn on the figure is an approximate envelope for the new zone; however, since the two zones are rather disjoint, at least for small E, the bounding line happens to fall within the canyon.

In conclusion, we have shown that the term responsible for the instability is that of the interaction of the base-state polymer stresses with the gradients of the disturbance velocity. Furthermore the simple oscillator model equation captures the mechanism of the new viscoelastic instability both *qualitatively* and *quantitatively*. In the next section we will provide a physical picture of the underlying mechanism.

6.3. *Physical mechanism*

In this section we provide a physical interpretation of the mathematical solution of our model equation. The equation is rewritten, without the damping term:

$$\ddot{\zeta} + \frac{1}{Re}(\boldsymbol{k}\cdot\boldsymbol{A}\cdot\boldsymbol{k})\zeta = 0. \tag{77}$$

A simple recasting of the equation proves quite illuminating:

$$\ddot{\zeta} + \left(\frac{1}{Re}\hat{\boldsymbol{k}}\cdot\boldsymbol{A}\cdot\hat{\boldsymbol{k}}\right)k^2\zeta = 0, \tag{78}$$

where $\hat{\boldsymbol{k}}$ denotes the unit vector in the direction of the wavevector. The quantity in parentheses is the 'normal' component of the basic-state stress, in the direction of propagation of the wave. Therefore we need to investigate the nature of this time-dependent 'normal' stress. To gain insight into the behaviour of tensor $\boldsymbol{A}$ we will determine its principal values and principal directions. The eigenvalues, λ, of $\boldsymbol{A}$ are

$$\lambda = \frac{\dot{\Gamma}}{1+4De^2}\left[-De(E-E^{-1}) \pm (1+De^2(E+E^{-1})^2)^{1/2}\right]. \tag{79}$$

A good feel for these expressions is developed if one considers the two limits of small and large De. Then the eigenvalues and the corresponding eigenvectors $\boldsymbol{l}$ are

$$De \to 0: \begin{cases} \lambda_+ = \dfrac{\dot{\Gamma}}{1+4De^2}[-1-De(E-E^{-1})], & \boldsymbol{l}_+ = \begin{Bmatrix} 1 \\ -1+De(E+E^{-1}) \end{Bmatrix} \quad \underbrace{\longleftrightarrow}_{\text{tension}} \\ \lambda_- = \dfrac{\dot{\Gamma}}{1+4De^2}[1-De(E-E^{-1})], & \boldsymbol{l}_- = \begin{Bmatrix} 1 \\ 1+De(E+E^{-1}) \end{Bmatrix} \quad \underbrace{\rightarrow\leftarrow}_{\text{compression}} \end{cases} \tag{80}$$

and

$$De \to \infty: \quad \begin{cases} \lambda_+ = -2DeE, & \boldsymbol{l}_+ = \begin{Bmatrix} 1 \\ 0 \end{Bmatrix} \quad \underbrace{\longleftrightarrow}_{\text{tension}} \\ \lambda_- = 2DeE^{-1}, & \boldsymbol{l}_- = \begin{Bmatrix} 0 \\ 1 \end{Bmatrix} \quad \underbrace{\rightarrow\leftarrow}_{\text{compression}} \end{cases} \tag{81}$$

(recall $\dot{\Gamma} < 0$). Therefore, depending on the relaxation time scale of the polymer, the compression and stretch axes (subscripts '—' and '+', respectively) are displaced either slightly by an amount proportional to De for small De, or by as much as $\pi/4$ from the corresponding compression and extension axes for the base-flow shear, which themselves always lie at $\pm\pi/4$. The trend is intuitively pleasing. However, for the dynamics problem at hand, the important conclusion of this exercise is the observation that there is a tensile and a compressive principal stress generated by the polymer.

The physical mechanism of the instability can now be stated. Recall that the incompressibility of the flow requires the disturbances to be transverse waves ($\boldsymbol{k}\cdot\boldsymbol{u} = 0$). Therefore as the wavevector rotates through its orbit, the direction of propagation samples both the tensile and the compressive directions. The transverse nature of the waves causes the polymer stress to become wavy. When the unperturbed stressed polymers are under tension, the curvature induced by the k^2-term of the passing wave in (78) results in a restoring force which opposes the disturbed configuration of the polymer; this is the stabilizing phase of the motion. However, as the wavevector gets aligned with the compressive direction, then the polymers are compressed in the direction of propagation of the disturbance wave. As the polymers feel the transverse disturbance of the passing wave, they simply buckle, in analogy to negative surface tension in a membrane. The question of stability is then one of the net destabilization the polymers feel during each rotational cycle of the wavevector. Clearly the instability is a secular one: it builds up over time; however, the timescale over which the growth occurs is inertial and can be rather explosive. The parameters of the problem determine whether the flow remains stable or goes unstable. Unfortunately, as can be seen from the forms of the stability diagrams presented throughout this article, or from the form of the classical Mathieu diagram, one's intuition is not sufficient to decide *a priori* whether a given parameter range will correspond to stability or instability.

Once the mathematical solution clarifies the stability response of the system, then the mechanism is that stated here.

6.4. *Summary*

In summary, the addition of viscoelasticity gives rise to new modes of instability in addition to the known inertial ones. These are plane waves whose rotating wavevector propagates at almost normal angles (as well as a completely normal angle) to the vortex axis. The physical mechanism is completely different from the inertial instability. All that is needed is the periodicity of the base flow and the rotation of the disturbance wavevector. The rest is solely due to the contribution of the polymers. If the base flow is such that the polymers feel a linear straining motion and experience tension in some directions and compression in other directions, then the passage of a transverse disturbance wave through each of those directions will give rise to stabilization and destabilization, respectively. Which one eventually prevails over the cycle can only be obtained from the solution of the mathematical equations. This mechanism can be expected to be of generic relevance to many other polymeric flows.

This work was accomplished during H.H.-H.'s sabbatical visit to Stanford University. H.H.-H. was supported on a Sesquicentennial Fellowship through the Edgar F. Shannon Jr. Center for Advanced Studies at the University of Virginia during his sabbatical leave. H.H.-H. acknowledges further support through the NSF and the Office of Microgravity Science at NASA. Last and not least, H.H.-H. acknowledges the gracious hospitality of his host and colleague, G.M.H. G.M.H. acknowledges the support of the US Department of Energy, Office of Basic Energy Sciences.

Appendix. Entries of the matrix Floquet equation

Let $\bar{R} \equiv Re/\bar{\kappa}$, $R \equiv Re/\kappa$, $S_1 \equiv (-2E\ Dek_1 + k2)\dot{\Gamma}$, and $S_2 \equiv (2Dek_2/E + k_1)\dot{\Gamma}$.

$$
\begin{array}{lll}
C_{11} = -2k_1k_2/(Ek^2) + R(k^2-k_1^2) & C_{12} = E(2k_1^2/k^2-1) - Rk_1k_2 & C_{13} = -Rk_1k_3 \\
C_{14} = -\bar{R}k_1(1-k_1^2/k^2) & C_{15} = \bar{R}k_1k_2^2/k^2 & C_{16} = \bar{R}k_1k_3^2/k^2 \\
C_{17} = \bar{R}k_2(-1+2k_1^2/k^2) & C_{18} = \bar{R}k_3(-1+2k_1^2/k^2) & C_{19} = \bar{R}2k_1k_2k_3/k^2 \\
 & & \\
C_{21} = -(2k_2^2/k^2-1)/E - Rk_1k_2 & C_{22} = 2Ek_1k_2/k^2 + R(k^2-k_2^2) & C_{23} = -Rk_2k_3 \\
C_{24} = \bar{R}k_1^2k_2/k^2 & C_{25} = -\bar{R}k_2(1-k_2^2/k^2) & C_{26} = \bar{R}k_2k_3^2/k^2 \\
C_{27} = \bar{R}k_1(-1+2k_2^2/k^2) & C_{28} = \bar{R}2k_1k_2k_3/k^2 & C_{29} = \bar{R}k_3(-1+2k_2^2/k^2) \\
 & & \\
C_{31} = -2k_2k_3/k^2 - Rk_1k_3 & C_{32} = 2Ek_1k_3/k^2 - Rk_2k_3 & C_{33} = R(k^2-k_3^2) \\
C_{34} = \bar{R}k_1^2k_3/k^2 & C_{35} = \bar{R}k_2^2k_3/k^2 & C_{36} = -\bar{R}k_3(1-k_3^2/k^2) \\
C_{37} = \bar{R}2k_1k_2k_3/k^2 & C_{38} = \bar{R}k_1(-1+2k_3^2/k^2) & C_{39} = \bar{R}k_2(-1+2k_3^2/k^2) \\
 & & \\
C_{41} = 2S_1 + 2k_1/De & C_{42} = 0 & C_{43} = 0 \\
C_{44} = 1/De & C_{45} = 0 & C_{46} = 0 \\
C_{47} = 2E & C_{48} = 0 & C_{49} = 0 \\
 & & \\
C_{51} = 0 & C_{52} = 2S_2 + 2k_2/De & C_{53} = 0 \\
C_{54} = 0 & C_{55} = 1/De & C_{56} = 0 \\
C_{57} = -2/E & C_{58} = 0 & C_{59} = 0
\end{array}
$$

$$
\begin{array}{lll}
C_{61} = 0 & C_{62} = 0 & C_{63} = 2k_3/De \\
C_{64} = 0 & C_{65} = 0 & C_{66} = 1/De \\
C_{67} = 0 & C_{68} = 0 & C_{69} = 0 \\
 & & \\
C_{71} = S_2 + k_2/De & C_{72} = S_1 + k_1/De & C_{73} = 0 \\
C_{74} = -1/E & C_{75} = E & C_{76} = 0 \\
C_{77} = 1/De & C_{78} = 0 & C_{79} = 0 \\
 & & \\
C_{81} = k_3/De & C_{82} = 0 & C_{83} = S_1 + k_1/De \\
C_{84} = 0 & C_{85} = 0 & C_{86} = 0 \\
C_{87} = 0 & C_{88} = 1/De & C_{89} = E \\
 & & \\
C_{91} = 0 & C_{92} = k_3/De & C_{93} = S_2 + k_2/De \\
C_{94} = 0 & C_{95} = 0 & C_{96} = 0 \\
C_{97} = 0 & C_{98} = -1/E & C_{99} = 1/De
\end{array}
$$

REFERENCES

Azaiez, J. & Homsy, G. M. 1994*a* Linear stability of free shear flow of viscoelastic liquids. *J. Fluid Mech.* **286**, 37–69.

Azaiez, J. & Homsy, G. M. 1994*b* Numerical simulation of non-Newtonian free shear flows at high Reynolds numbers. *J. Non-Newtonian Fluid Mech.* **52**, 333–374.

Batchelor, G. K. 1967 *An Introduction to Fluid Dynamics*. Cambridge University Press.

Bayly, B. J. 1986 Three-dimensional instability of elliptical flow. *Phys. Rev. Lett.* **57**, 2160–2163.

Bayly, B. J., Orszag, S. A. & Herbert, Th. 1988 Instability mechanisms in shear-flow transition. *Ann. Rev. Fluid Mech.* **20**, 359–392.

Berman, N. 1978 Drag reduction by polymers. *Ann. Rev. Fluid Mech.* **10**, 47–64.

Bird, R. B., Curtiss, C. F., Armstrong, R. C. & Hassager, O. 1987 *Dynamics of Polymeric Liquids*. vol. 2, 2nd edn. Wiley-Interscience.

Bonn, D., Couder, Y., Dam, P. H. J. van & Douady, S. 1993 From small scales to large scales in three-dimensional turbulence: The effect of diluted polymers. *Phys. Rev.* E **47**, R28–R31.

Greenspan, H. P. 1968 *The Theory of Rotating Fluids*. Cambridge University Press.

Grimshaw, R. 1990 *Nonlinear Ordinary Differential Equations*. Blackwell Scientific Publications.

Herbert, Th. 1988 Secondary instability of boundary layers. *Ann. Rev. Fluid Mech.* **20**, 487–526.

Ho, C. M. & Huerre, P. 1984 Perturbed free shear layers. *Ann. Rev. Fluid Mech.* **16**, 365–424.

Kachanov, Y. S. 1994 Physical mechanisms of laminar-boundary-layer transition. *Ann. Rev. Fluid Mech.* **26**, 411–482.

Pierrehumbert, R. T. 1986 Universal short-wave instability of two-dimensional eddies in an inviscid fluid. *Phys. Rev. Lett.* **57**, 2157–2159.

Stuart, J. T. 1967 On finite amplitude oscillations in laminar mixing layers. *J. Fluid Mech.* **29**, 417–440.